Materials Science & Engineering C 96 (2019) 391–401

Contents lists available at ScienceDirect

Materials Science & Engineering C

journal homepage: www.elsevier.com/locate/msec

Synthesis, characterization and application of Ag doped ZnO nanoparticles in a composite resin☆

Hércules Bezerra Dias[a,c], Maria Inês Basso Bernardi[a], Valéria Spolon Marangoni[a], Adilson César de Abreu Bernardi[b], Alessandra Nara de Souza Rastelli[c,*], Antônio Carlos Hernandes[a]

[a] University of São Paulo - USP, Physics Institute of São Carlos – IFSC, Department of Physics and Materials Science, São Carlos, São Paulo 13566-590, Brazil
[b] University of Araraquara – UNIARA, School of Biomedicine, Department of Biology and Health Sciences, Araraquara, São Paulo 14801-340, Brazil
[c] University of São Paulo State – UNESP, Araraquara School of Dentistry, Department of Restorative Dentistry, Araraquara, São Paulo 14801-903, Brazil

ARTICLE INFO

Keywords:
Nanoparticles
Zinc oxide
Silver
Antibacterial agent
Biofilms
Dental caries
Streptococcus mutans

ABSTRACT

The biofilm accumulation over the composite resin restorations can contribute to the formation of secondary caries. In this way, antibacterial restorative composite resins are highly desired. Then, the purpose of this study was to modify a composite resins using Ag doped ZnO nanoparticles (NPs), evaluate the antibacterial and mechanical properties of the modified composite resin. The ZnO/AgNPs were synthesized by two different routes, polymeric precursor and coprecipitation methods, and characterized by thermal decomposition, X-ray diffraction, specific surface area by N_2 desorption/desorption and scanning electron microscopy (SEM). Antibacterial activity of composite resin specimens (4 mm in height and 2 mm in diameter; n = 15) modified by ZnO/Ag nanoparticles was performed against 7-days *Streptococcus mutans* biofilm. Colony forming units (CFU/mL) were used to evaluate the bacterial activity. Additionally, the morphology and the bacteria adherence area were analyzed by SEM images. Cylindrical specimens (6 mm in height and 4 mm in diameter; n = 20) of the composite resin containing ZnO/Ag NPs were prepared to perform compressive strength in a universal mechanical test machine, and the surface of fractured specimens was analyzed by EDX element mapping to verify NPs homogeneity. The normal distribution was confirmed and the two-way analysis of variance (ANOVA) and Tukey's test for pair comparison were performed. The nanospheres of ZnO/Ag lead to a better biofilm inhibition, than nanoplates. No difference on compressive strength was found for the composite resin modified by ZnO/Ag nanoplates. Based on these results, this material could be a good option as a new restorative material.

1. Introduction

Secondary caries have been described as an important reason for composite resin restoration failure and can occurs mainly due the accumulation of biofilm on the surface of dental restorative materials, resulting on the need of replacement of restorations [1,2]. Replacement dentistry is costly. In 2005, the annual cost for dental fillings in the United States was $46 billion [3]. Composite resins have grown popular for tooth cavity restorations mainly due their esthetics and direct-filling capabilities [4–7]. Although the physical and mechanical properties of composite resins have been significantly improved in the last years [8–11], these materials tend to accumulate more biofilm than other restorative materials [12].

Antimicrobial agents have been incorporated into the composite resins to reduce or inhibit biofilm formation [13]. Among them, agents such as silver (Ag) [14,15] or silver ion-implanted fillers [16] have been demonstrated good antimicrobial activity without significant changes on the mechanical properties of the composite resin.

Nanotechnology is on the verge of initiating extraordinary advances in biological and biomedical sciences. Also, the nanotechnologies are predicted to revolutionize the control over materials properties at ultrafine scales and the sensitivity of tools and devices applied in several scientific and technological fields [17]. In the dental field, nanotechnology has been applied as an innovative concept for the development of materials with better properties and anticaries potential [18].

☆ The author(s) declare(s) that there is no conflict of interest regarding the publication of this paper.

* Corresponding author at: São Paulo State University - UNESP, Araraquara School of Dentistry, Department of Restorative Dentistry, 1680 Humaita St., Mail Box: 331, Araraquara, São Paulo 14.801-903, Brazil.
E-mail addresses: m.basso@ifsc.usp.br (M.I.B. Bernardi), alrastelli@foar.unesp.br (A.N. de Souza Rastelli), hernandes@ifsc.usp.br (A.C. Hernandes).

https://doi.org/10.1016/j.msec.2018.10.063
Received 28 December 2017; Received in revised form 3 September 2018; Accepted 16 October 2018
Available online 17 October 2018
0928-4931/ © 2018 Elsevier B.V. All rights reserved.

Table 1
Ag doped and undoped ZnO nanoparticles synthetized by two methods.

Sample	Synthesis route	% Ag (mass)	T (°C) and time (min) Calcination 1	T (°C) and time (min) Calcination 2
ZPS	PolymPrec[a]	0.1	300/240	500/120
ZCS	Coprecip[a]	0.1	–	–

[a] PolymPrec: polymeric precursors synthesis; Coprecip: coprecipitation synthesis.

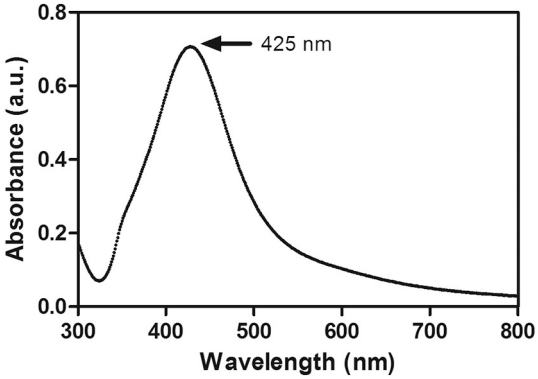

Fig. 1. The UV–Visible spectrometry of Ag nanoparticles.

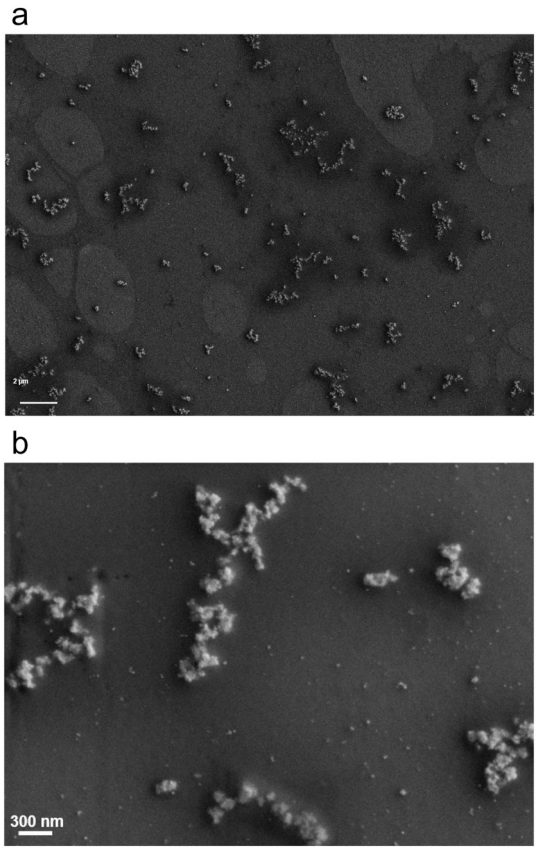

Fig. 2. Scanning electron microscopy images of Ag nanoparticles.

Metal oxides such as silica, zirconia, and alumina have been used to increase the strength of restorative materials based on composite resins [19]. Other metal oxides, such as zinc oxide (ZnO) have also been incorporated as opaque reinforcing fillers into composite resins [20,21]. Moreover, ZnO and several other oxides have shown good antimicrobial effect against oral microorganisms that contribute to the dental caries [22]. The use of metal oxides nanoparticles (NPs) have been found to be more effective than larger particles against both gram negative and gram positive bacteria [23,24].

The use of silver-decorated materials has been recently demonstrated a high efficient strategy against biofilm infections, including that caused by oral pathogens such as *Candida albicans*, *Lactobacillus acidophilus*, *Streptococcus mutans*, and *Aggregatibacter actinomycetemcomitans* [25,26]. The synergetic antibacterial effect of nanohybrid or nanocomposites (ZnO/Ag) has found to be more effective against Gram-positive and Gram-negative bacteria, compared with their individual components [15,27,28]. The association of ZnO and Ag nanoparticles is capable to increase ROS (reactive oxygen species) production and enhance bacterial activity [15,27]. The inclusion of an antibacterial nanohybrid material into a resin based restorative material could inhibit the oral biofilm formation over the surface of restorations, contributing to prevention of secondary caries [29].

The goal of this study was synthetize and characterizes nanoparticles (Ag decorated ZnO nanoparticles) to modify a commercial composite resin, which was designed with special end-use properties such as antibacterial effects. The blended composite resin was examined regarding inhibition of *Streptococcus mutans* biofilm and compressive strength.

2. Materials and methods

2.1. Synthesis of silver nanoparticles

Silver (Ag) nanoparticles were prepared using polyvinyl alcohol (PVA, 99.0%), sodium borohydride (NaBH4, 99.0%) and silver nitrate ($AgNO_3$, 99.9%) [30]. All reagents were purchased from Sigma Aldrich Inc. (USA) and used without any further purification. All solutions were prepared with ultrapure water (Milli-Q, 18.2 MΩ·cm at 25 °C). Briefly, PVA (0.010 g) was diluted with 20 mL of water heated at 80 °C and reserved. Simultaneously, a 0.1 mol L^{-1} solution of $NaBH_4$ and $AgNO_3$ (7 mg in 40 mL of water) were prepared. The PVA and $AgNO_3$ solutions were mixed and stirred for 2 min, followed by adding 1 mL of $NaBH_4$ solution.

2.1.1. Synthesis of ZnO by polymeric precursor method and ag doping

The polymeric precursor method is based on the polymerization of metallic citrate using ethylene glycol. A hydrocarboxylic acid such as citric acid is normally used to chelate cations in an aqueous solution. The addition of a polyalcohol such as ethylene glycol leads to the formation of an organic ester. Polymerization promoted by heating around 100 °C results in a homogenous resin in which the metal ions are uniformly distributed throughout the organic matrix. The resin is then calcined to produce the desired oxides [31].

Zinc nitrate ($Zn(NO_3)_2{\cdot}6H_2O$, Sigma Aldrich Inc. USA), and citric acid ($C_6H_8O_7{\cdot}H_2O$, 99.5%, Synth) were used as precursors. The citric acid:metal ratio was 3:1. The zinc nitrate, citric acid, and dopants were dissolved in water and then mixed into an aqueous citric acid solution (100 °C) under constant stirring. For Ag doping (0,1% mass), the suspension was added in this order. Next, ethylene glycol ($HOCH_2CH_2OH$, P.A. > 99,5%, Synth) was added to polymerize the citrate by a polyesterification reaction. The ethylene glycol:citric acid (EG:CA) mass ratio was 40:60. The resulting resin was calcined at 300 °C for 4 h at 10 °C/min, leading to the formation of the precursors powder. The data sample (ZPS–Ag doped ZnO NPs) was showed in Table 1.

2.1.2. Synthesis of ZnO by coprecipitation method and Ag doping

The zinc nitrate hexahydrate ($Zn(NO_3)_2{\cdot}6H_2O$, Sigma Aldrich Inc. USA) and sodium hydroxide (NaOH, Merck) were of analytical grade and used without further purification. In a typical synthesis process, 1.5 g of $Zn(NO_3)_2{\cdot}6H_2O$ was dissolved in a mixture of 300 mL of deionized water (solution 1) and 2 g of NaOH was dissolved in 10 mL of

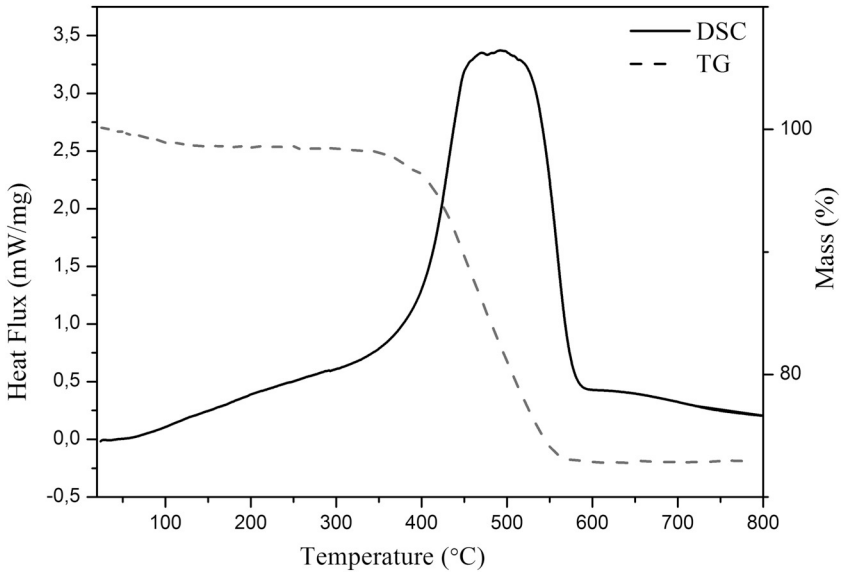

Fig. 3. Thermogravimetry (TG) and differential scanning calorimetry (DSC) of ZPS sample–Ag/ZnO (500 °C/0.1% Ag).

deionized water to obtain another solution (solution 2). Under vigorous stirring, solution 2 was poured into solution 1 at room temperature, and the mixture was kept under vigorous stirring during the reaction process. For Ag doping (0.1% mass), the suspension was added in this order. After being further stirrer for 6 h, the white precipitates were collected by centrifugation and washed with deionized water repeatedly until neutral pH [32]. The precipitates were then dried at 60 °C for 24 h. The data sample (ZCS-Ag doped ZnO) is shown in Table 1.

2.2. Characterization of the nanoparticles

The samples were structurally characterized using an automatic X-ray diffractometer (Rigaku, Ultima IV) with CuKα radiation (40 kV, 46 mA, θ = 1.5405 Å) and in a θ − 2θ configuration using a graphite monochromator. The scanning range was between 20 and 80° (2θ), with a step size of 0.02° and a step time of 1.0 s.

The thermal decomposition processes were evaluated by thermogravimetry (TG, Netzsch STA 409C), under an oxygen atmosphere at a heating rate of 10 °C/min. The Al_2O_3 was used as reference material during the thermal analysis.

The microstructural characterization of ZnO NPs was carried out under a high resolution field emission gun scanning electron microscopy (FEG-SEM Supra 35, Zeiss, Germany) operating at 3 kV.

The synthesis of Ag NPs was monitored by UV–Visible spectrometry, carried out using a Hitachi U-2900 spectrometer using a 1 cm quartz cell. The size and morphology of the PVA-stabilized Ag NPs was carried out under a high resolution field emission gun scanning electron microscope - FEG-SEM (Zeiss) at 2.0 kV. For this, diluted samples of the suspension were deposited in silicon substrates and dried at room temperature.

The specific surface area (BET) was estimated from the N_2 desorption/adsorption isotherms at liquid nitrogen temperature, using a Micrometrics ASAP 2020.

2.3. Composite resin modification

The ZnO/Ag nanoparticles were added into the composite resin using a standardized protocol based on the inclusion of weight percentage of nanoparticles into the composite resin [33]. Briefly, after weighed of nanoparticles corresponding to 1 and 2% in weight, these amounts were incorporated into the composite resin by manual mixture for 1 min, using a metal spatula and a glass plate. In order to confirm the homogeneity of nanoparticles into the composite resin, scanning electron microscopy with an energy dispersive X-ray analytical system (SEM-EDX) was performed on the fractured surface of samples for each experimental group.

2.4. Antibacterial activity

2.4.1. Bacterial strain and growth conditions

Streptococcus mutans strain ATCC 25175 provided by Fiocruz Foundation (Department of Microbiology, Reference Materials Laboratory, Sector Reference Bacteria located in the Oswaldo Cruz Foundation, National Institute of Health Quality Control -. INCQS, Av Brazil, 4365 - Manguinhos, Cep: 21045-900, Rio de Janeiro, RJ, Brazil) was used in this study. Initially, 3 to 5 colonies were collected from the Petri dish containing BHI agar (Brain Heart Infusion, Difco Laboratories, Becton Dickinson and Company, USA) + 1% sucrose, placed in a 15 mL falcon tube containing 5 mL of Bacto™ BHI broth + 1% sucrose and incubated at 37 °C (± 1 °C) for 18 h. After growing, the bacterial culture was centrifuged (Excelsa® II Centrifuge, FANEM, Mod. 206 BL, serial number: HV 9462) at 3000 rpm for 15 min to obtain the pellet. The supernatant was discarded and the pellet resuspended in PBS (phosphate buffered saline) until reaching the absorbance of 0.08 read at 600 nm, with amount of cells in the order of 10^8 CFU/mL using a spectrophotometer (Eppendorf AG, Hamburg, Germany).

2.4.2. Biofilm formation and bacterial counting

The composite resin specimens (4 mm in height and 2 mm in diameter; n = 15) were placed in a 24-wells microculture plates (Nunclon™, Nunc) and the wells were filled with 100 μL of *Streptococcus mutans* in a BHI suspension plus 900 μL of BHI broth supplemented with 1% sucrose. Then, the plates were incubated at 37 °C (± 1 °C) for 7 days. The BHI broth solution containing 1% of sucrose was replaced every 48 h. After 7 days, the BHI broth solution was removed, and the specimens were washed with sterile phosphate-buffered saline (PBS) for three times to remove non-adherent cells. The specimens were placed into sterile test tubes containing 5 mL of PBS (phosphate-buffered saline) solution, stirring using a vortex for 1 min and immersed in an ultrasonic bath (Cristófol Equipamentos de Biossegurança Ltda, Campo Mourão, Paraná, Brasil) during 5 min (room temperature; 42 kHz; 160 W). After that, the serial dilution was performed. From the initial

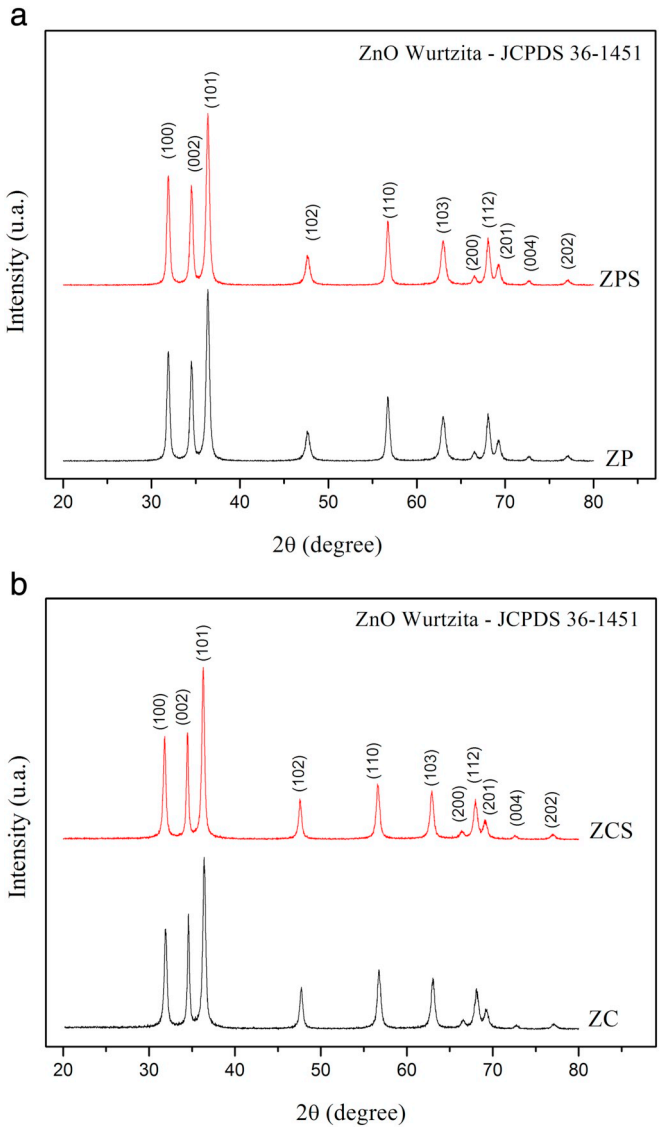

Fig. 4. XRD patterns of Ag/ZnO NPs synthesized by (a) polymeric precursor: ZPS (500 °C / 0.1% Ag); (b) coprecipitation: ZCS (0.1% Ag) at room temperature.

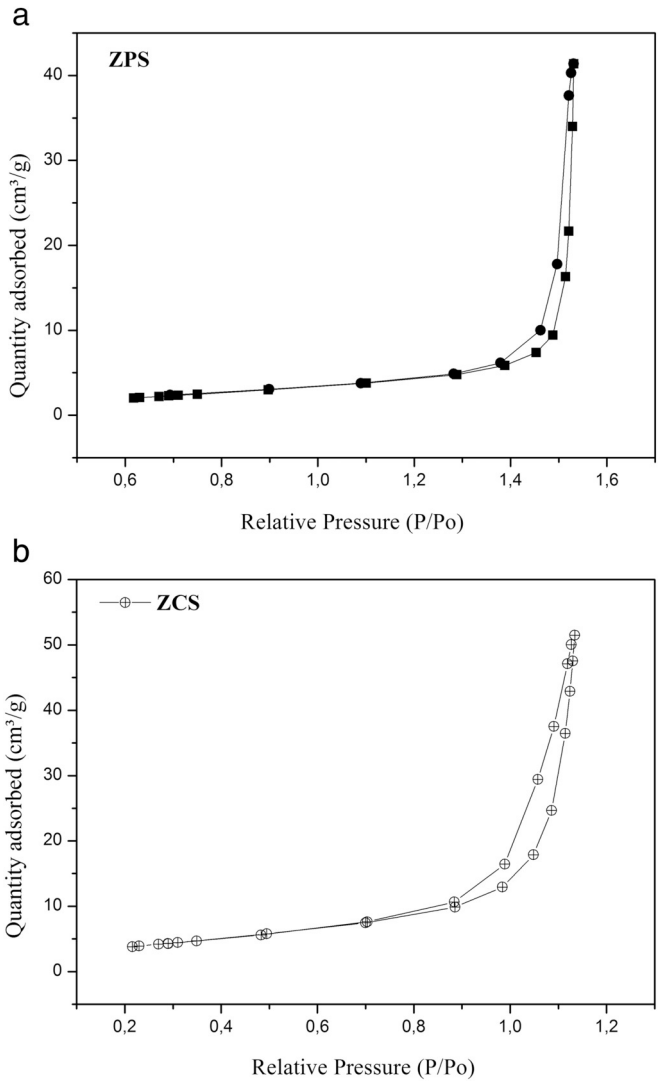

Fig. 5. N_2 adsorption-desorption isotherms of Ag/ZnO NPs synthesized by (a) polymeric precursor: ZPS (500 °C/0.1% Ag); (b) coprecipitation: ZCS (Ag 0.1% at room temperature).

solution, five sequential solutions were obtained and aliquots of 25 μL from each tube were seeded on brain-heart infusion agar plates and incubated at 37 °C (± 1 °C) for 48 h, and then the colony forming units (CFU/mL) were counted.

After the incubation, the plates with 30 to 300 typical colonies of *S. mutans* were counted in a colony counter (Phoenix CP-600, São Paulo, Brazil), and mean values of CFUs were obtained (CFU/mL).

2.4.3. Microscopy biofilm analysis

After biofilm formation over the composite resins specimens for seven days and washing procedures using PBS solution, as previously described, the specimens were placed into a new 24-wells microculture plate and immersed in 1 mL of 2.5% glutaraldehyde solution during 15 min for fixation of the bacteria. Then, the specimens were dehydrated in an increasing series of absolute alcohol (ethanol ≥ 99,8%, Sigma Aldrich) 15, 30, 50, 70, 90 and 100% for 15 min each, dried under room temperature and the surfaces were gold sputter coated. The SEM (scanning electron microscopy) analysis was performed using a scanning electron microscopy with an energy dispersive X-ray analytical system (SEM-EDX, F50 FEI, Nederland).

2.4.4. Determination of the bacterial cell adhesion area

The SEM images of the biofilm formed over the surface of composite resin specimens containing ZnO/Ag NPs were analyzed by image edition software (Image J 1.48V, Wayne Rasband National Institute of Health, USA), in order to determine the corresponding area of the bacterial cell adhesion for each group. Using image contrast method, eight images of each group were compared, at the same magnification, according to the percentage of the cells adhered to the surface of the specimens, and then the values were calculated.

2.5. Compressive strength test

For the compressive strength test, cylindrical specimens of composite resin Filtek™ Z350XT (3M do Brasil, lot number: 726707) were prepared for the four experimental groups. Eight composite resin specimens were prepared for each group, modified by 1 and 2% (wt%) of Ag/ZnO NPs and unmodified with NPs (control group). The specimens (n = 40) were prepared using a stainless steel split mold (4 mm in diameter and 6 mm in height) according to ANSI ADA specification n.27 (American National Standard, 1993) placed on a glass slide and then overfilled with the composite resin doped with nanoparticles. After complete filling of the mold, another glass slide was pressed on the top

Table 2
Surface area, crystallite and particle diameter of ZnO and Ag/ZnO NPs.

Sample	Surface area (m^2/g)	Particle diameter (nm) by SEM images	Particle diameter (nm) by BET	Crystallite diameter (nm)
ZPS	42.26	23 ± 4	25	23
ZCS	16.80	10 ± 4[a]	63	24

[a] Nanoplates diameter.

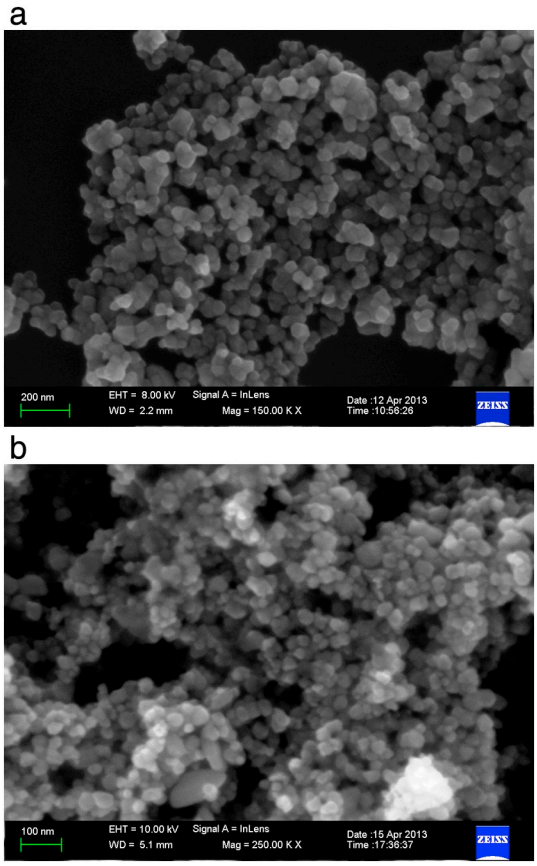

Fig. 6. Scanning electron microscopy images of Ag/ZnO NPs synthesized by polymeric precursor method: ZPS (500 °C/0.1% Ag).

surface and the whole material light-cured during 40 s using a blue LED (Radii Plus - SDI, Australia, Serial number: 52270, Part Number: 5600052) on the top and bottom surfaces. After removal of the mold, the lateral sides of the specimens were light-cured for further 40 s in order to achieve high polymerization. The specimens were stored in distilled water at 37 °C (± 1 °C) for 24 h prior to test. The compressive strength was performed employing a mechanical test machine (DL2000, EMIC - Equipamentos e Sistemas de Ensaio Ltda., São José dos Pinhais, Paraná - Brazil) with a load cell of 5 kN at a cross-speed of 0.5 mm·min^{-1}. The specimens were placed with their flat ends between the plates of the testing machine so that the progressively increasing compressive load was applied along the long axis of the specimens. The software Tesc (Test Scipt, EMIC - Equipamentos e Sistemas de Ensaio Ltda., São José dos Pinhais, Paraná - Brazil) performed data recording and processing for compressive strength values. The fractured specimens obtained from mechanical test were submitted to EDX (Supra 35, Zeiss, Germany). The samples were mounted on the aluminum stub using carbon-coated double sided adhesive tape and then coated with gold using sputter coater. The distribution of ZnO/Ag NPs in composite resin specimens was analyzed by EDX elemental composition (2.0×10^{-9} A, 30 kV, spot size of 500 nm and 100 s).

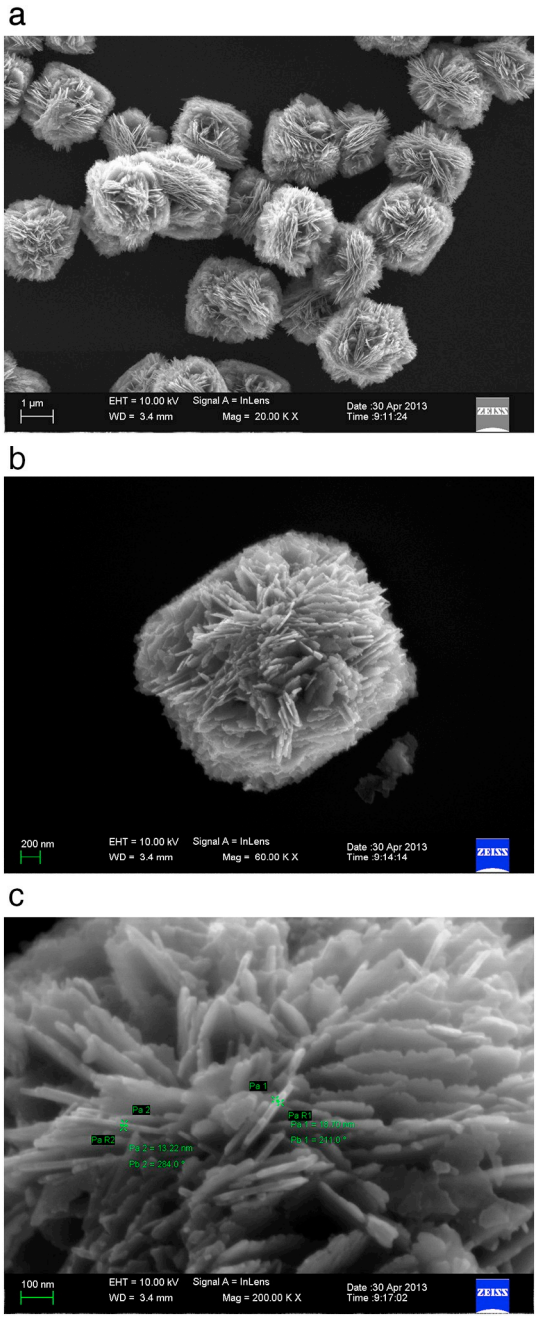

Fig. 7. Scanning electron microscopy images of (a–c) Ag/ZnO (ZCS-0.1% Ag) synthesized by coprecipitation at room temperature.

2.6. Statistical analysis used

The normal distribution and homoscedasticity were analyzed by Shapiro–Wilk and Levene tests. Viable cells of the 7-days biofilm by CFU/mL, bacteria adhesion and compressive strength means values according to the amount of the nanoparticle and synthesis method used

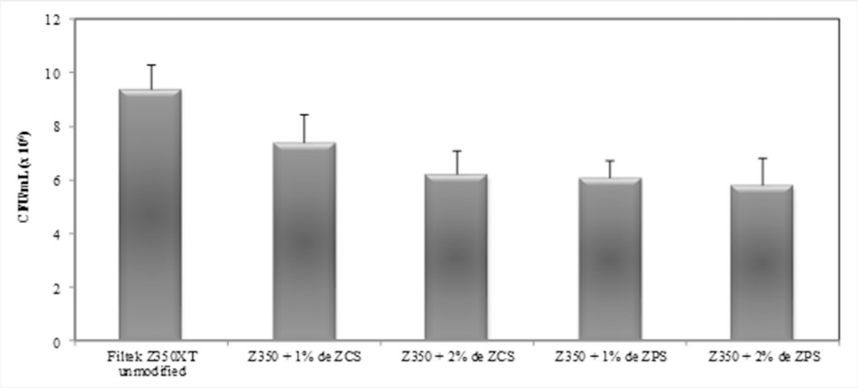

Fig. 8. CFU/mL of *S. mutans* biofilm (mean values and standard deviation) after seven days incubation on: unmodified and modified composite resin containing 1% and 2% of Ag/ZnO NPs, respectively.

was performed by two-way analysis of variance (ANOVA). Multiple comparisons were performed using Tukey's test. The analyses were performed using the software IBM SPSS Statistics 20.0 (SPSS Inc. Chicago, USA) at a significance level of 0.05.

3. Results

3.1. Synthesis and characterization of NPs

The UV–Vis spectroscopy revealed an absorbance peak at 425 nm (Fig. 1), characteristic of Ag nanoparticles [34]. The FEG-SEM images of PVA-Ag NPs (Fig. 2) revealed an average diameter around 10 nm.

The differential scanning calorimetry curves of the ZnO/Ag NPs, represented by sample ZPs (Fig. 3) was characterized by a multiple exothermic process, which is completed around 600 °C. The first thermal decomposition stage takes place at room temperature around 110 °C, which can be observed as a mass loss of 2% in thermogravimetry curve (Fig. 3) attributed to the removal of adsorbed water. In the next stage, and lead, thermal decomposition, ranging from 350 °C to 600 °C, a weight loss of 25% was observed. This mass loss was accompanied by highly exothermic broad peak in the DSC curve, a thermal decomposition stage associated to the total combustion of organic waste and subsequent crystallization of the crystalline phases.

The crystallinity and structure of the ZnO/Ag nanoparticles were confirmed by X-ray diffraction. As show in Fig. 4, the position and relative intensity of all diffraction peaks match well with the standard diffraction date for ZnO hexagonal structure (JCPDF file no. 36-1451). Characteristic peaks of impurity or peaks related to Ag were not observed due the low concentration of Ag.

Nitrogen adsorption-desorption isotherms were measured to determine the specific surface area of ZnO/Ag NPs, and the corresponding results are presented in Fig. 5. The isotherms can be assigned to type IV, corresponding to the presence of mesopores and characterized by the presence of hysteresis loop of type H1 - hysteresis 1, often associated with porous materials (agglomerates of uniform spheres in regular array with a very narrow pore size distribution) [32,35]. The specific superficial area, crystallite diameters and particle diameter estimated from SEM images and BET analysis are shows in Table 2.

Spherical particles with average diameter between 23 nm were obtained by polymeric precursors, while the coprecipitation synthesis provides nanoplates with 10 nm, as show in Table 2. The SEM images with morphologies of the nanoparticles are showed in Figs. 6 and 7. The inclusion of a small amount of Ag did not greatly influence the morphology and size of the synthesized nanostructures.

No difference in the average diameter of particle was noted, from BET measurements and by SEM images analysis for the ZnO/Ag NPs (ZPS sample), as shown in Table 1. However, differences were observed for the ZnO/Ag NPs (ZCS sample). This is due to the BET technique, that measures the surface area from agglomerated particles, while in the SEM images it is possible to distinguish isolate and agglomerated particles.

Fig. 8 shows the mean values for viable cells obtained by CFU/mL of 7-days *S. mutans* biofilm on unmodified and modified composite resin specimens by NPs. The specimens containing spherical nanoparticles of ZnO/Ag (ZPS sample) inhibited the growth of *S. mutans* biofilm cells in comparison to unmodified specimens, but no statistical significant differences were found ($p > 0.05$).

Fig. 9 shows SEM images of *S. mutans* biofilm induced over the surface of the unmodified and modified composite resin specimens with 1 and 2% of ZCS and ZPS NPs. It was possible to see a decrease in the amount of adhered cells on the specimens containing NPs in comparison to the unmodified composite specimens.

SEM images of biofilm analyzed by contrast using the software Image J were shown in Fig. 10. The reduction of the bacteria adhesion area on specimens containing NPs can be seen, confirming the results above. The results of bacterial cell adhesion area are showed in Fig. 11.

Fig. 12 shows the compressive strength of doped composite resin with NPs of ZnO/Ag, as well as undoped composite resin. The doped composite resin with 1 and 2% of ZnO/Ag NPs decreased compressive strength, except when modified with nanoplates (ZCS). No statistical significant difference was noted on compressive strength with addition of 1% ZCS ($p = 0.09$) and 2% ZCS ($p = 0.64$) NPs. Statistical significant difference was noted among the groups containing 1 ($p = 0{,}004$) to 2% (0,0001) of ZPS NPs in comparison to the unmodified composite resin.

4. Discussion

The polymeric precursors synthesis proposed by Pechini [36] has been used for decades to obtain different nanomaterials, including ZnO nanoparticles. The molar ratio EG:AC directly influences the size and morphology of ZnO and ZnO/Ag nanoparticles [37]. In this study, the molar ratio of EG:CA (4:6) produced crystalline ZnO/Ag nanospheres. The final chemical composition and morphology of nanostructures are also directly related to the concentration of zinc ions used in synthesis. The literature reports that the morphology of the ZnO nanostructures synthesized by coprecipitation at room temperature drastically changes with increasing concentration of zinc ions [32]. In this study, a citric acid:metal ratio of 3:1 successful produce three-dimensional ZnO/Ag nanostructures by coprecipitation method, as demonstrated by physical characterization (Figs. 1–7).

The antibacterial effect exhibited by the doped composite resin with ZnO/Ag nanospheres leads a better cell inhibition than ZnO/Ag nanoplates. This could be due to particle size and surface area, since ZPS nanoparticles showed surface area almost three times higher than the ZCS NPs. It is well known that the material type used to prepare the nanoparticles as well as the particle size are described as two important

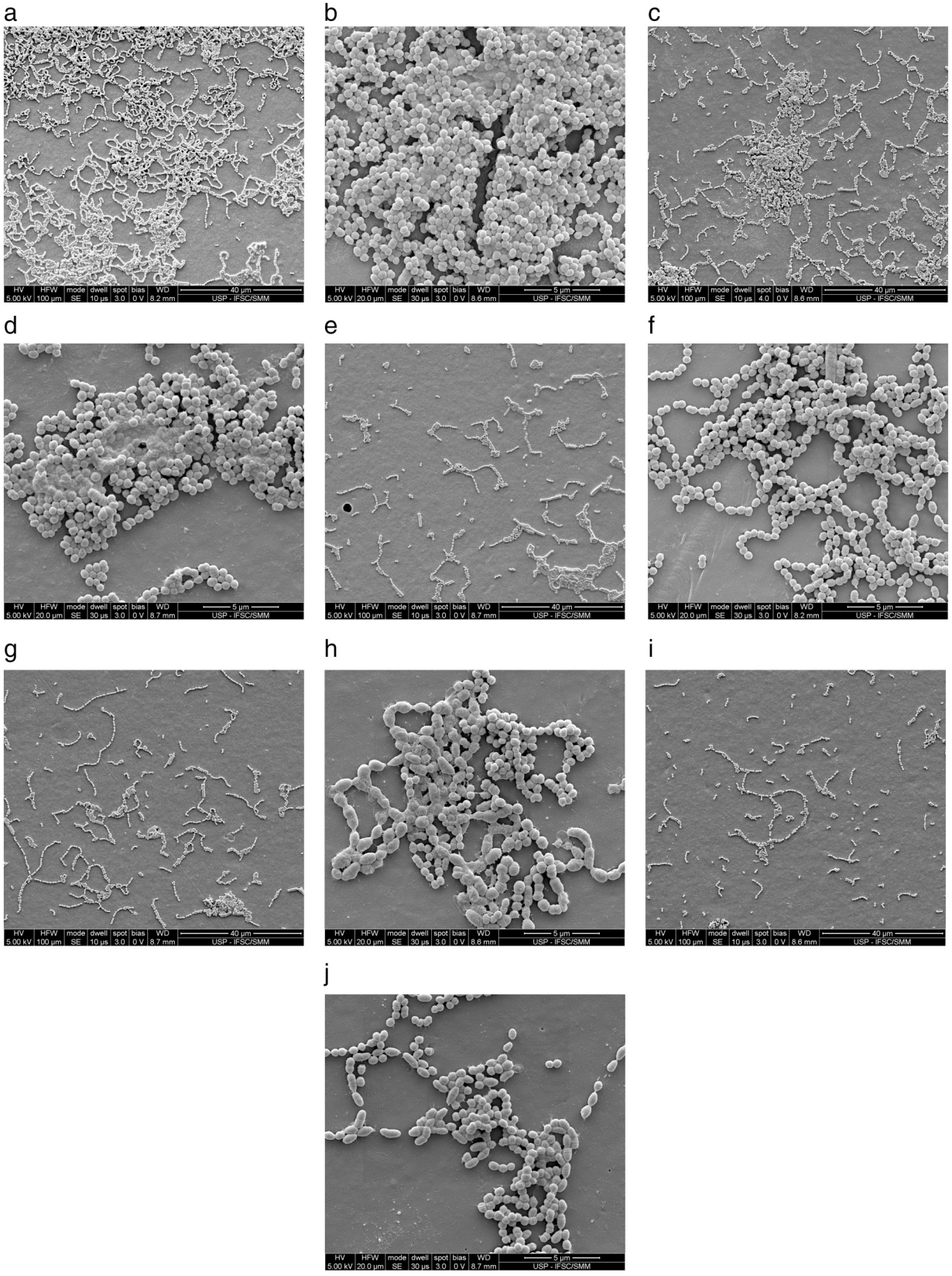

Fig. 9. SEM images of *S. mutans* mature biofilm adhered to unmodified (a–b), modified composite resin specimens with 1% of ZCS NPs (c–d), 2% of ZCS NPs (e–f), 1% of ZPS NPs (g–h) and 2% of ZPS NPs (i–j).

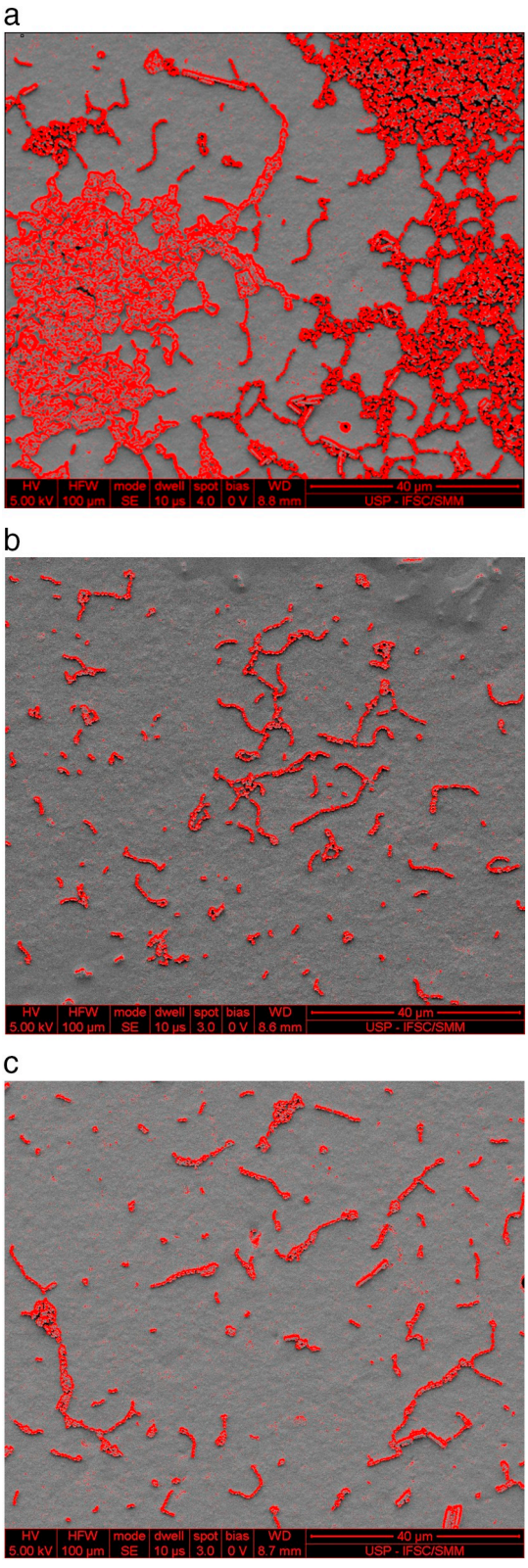

Fig. 10. Image J contrast analysis of SEM images (magnification: 2980×) for determination of adhesion area of the biofilm on (a) unmodified; (b) modified composite resin with 2% of ZPS NPs; and (c) with 2% of ZCS NPs, respectively. (For interpretation of the references to color in this figure legend, the reader is referred to the web version of this article.)

parameters that can affect the antibacterial effectiveness [38]. Hojati et al. [21] and Sevinç & Hanley [13] also reported the antibacterial ability of ZnO NPs after doped a composite resin.

The specific surface area value as well as the NPs concentration blended into the composite resin leads to the improvement of inhibitory effect over the biofilm, optimizing the ability of these materials to reduce the viability of bacterial cells [39]. As the particle size decreases, the surface area increases and this allows a greater amount of their atoms or molecules appears on the surface rather than inside the material. Clinical and experimental studies indicate that a small size, a large surface area and the ability to generate reactive oxygen species (ROS) provide to the nanomaterials the antibacterial ability [40]. Espinosa-Cristóbal et al. [41] reported antibacterial activity of Ag nanoparticles against *S. mutans* and describes that this property is dependent on the particle size, since smaller particles have greater inhibitory effect. The safe use of nanotechnology to control oral biofilms involves a full understanding of the interface between nanomaterials and biological systems [42].

Fig. 8 shows that the composite resins containing ZPS and ZCS NPs inhibited *S. mutans* biofilm better than undoped composite resin and the increased amount of NPs also improve this effect. Hojati et al. [21] related that the addition of ZnO NPs into flowable composite resin could significantly inhibit the growth of *S. mutans*. According to Kassaee et al. [43], the addition of small amounts of Ag NPs into a commercial acrylic resin provided a strong antibacterial effect with low toxicity to humans and improved the mechanical properties. Silver and zinc-silver supported materials were used to provide antibacterial effect against *S. mutans* and *Escherichia coli* in dental resin-based materials [44]. Kasraei et al. [16] also verified that composite resins containing silver or zinc oxide nanoparticles exhibited antibacterial activity against *Streptococcus mutans* (PTCC 1683) and *Lactobacillus* bacterial suspension (PTCC 1643).

In this study, it was found that small amounts of nanoplates and nanospheres of ZnO/Ag reduced the number of viable cells of the *S. mutans* biofilm. The bactericidal mechanism of Ag and ZnO is based on the disturbing of antioxidative system mainly by induction and accumulation of intracellular ROS and bacterial disruption due to the dissolution of Zn^{2+} ions, respectively [15,27]. Due to the strong interaction between metallic Ag and semiconductor ZnO, the ZnO/Ag nanohybrid shows enhanced and synergistic antibacterial activities for both Gram-negative and Gram-positive bacteria [27]. Jiang et al. [45] reported the potential antibacterial mechanisms of ZnO NPs, describing that both physical (Van der Waals forces, electrostatic, hydrophobic and receptor-ligand interactions) and chemical (dissolution of Zn^{2+} ions and ROS formation) interactions contributed to the antibacterial behavior of ZnO NPs. According to Zhang et al. [15], the association of Ag and ZnO NPs produces a synergetic enhanced of the bacterial activity inhibition. The enhanced antimicrobial activities of Ag-decorated materials toward oral pathogens was reported by Peng et al. [25], which attributed the best results to the dispersion of Ag NPs on the material surface.

The SEM images presented in Fig. 9 showed the adhesion of the *S. mutans* biofilm over the surface of composite resin specimens. The decrease on the surface adhesion of the biofilm was showed on the specimens containing ZnO/Ag NPs and the analysis using Image J software confirms that the inclusion of NPs reduced bacterial adhesion over the composite resin specimens, as demonstrated in Figs. 10–11. The biofilm is surrounded by an extracellular polysaccharide matrix that facilitates the formation of multicellular structures named micro colonies with high adherence ability to dental hard tissue surface or over dental restorative materials [24,46]. The literature reports that the biofilms are at least 500 times more resistant to antimicrobial products than

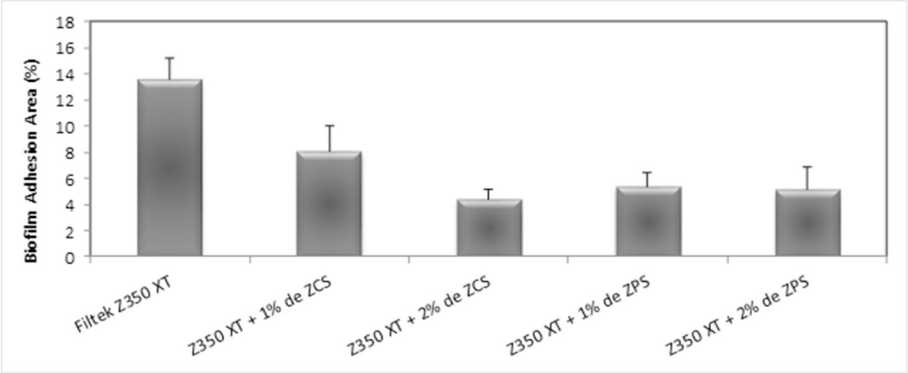

Fig. 11. Bacterial cell adhesion area estimated by the SEM images of *S. mutans* mature biofilm on the unmodified and modified composite resin specimens including 1% and 2% of Ag/ZnO NPs.

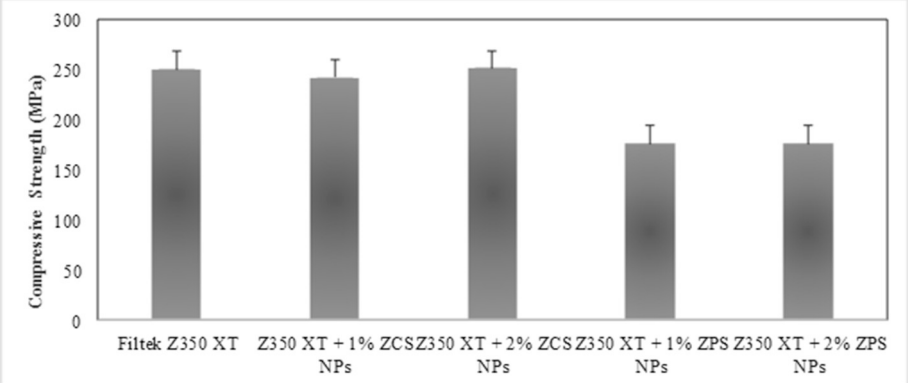

Fig. 12. Compressive strength mean values and standard deviations of unmodified and modified composite resin including 1 and 2% of Ag/ZnO NPs (ZCS and ZPS samples).

planktonic bacterial cells [47]. The 7-days biofilm incubation using in this current study, is considered a mature biofilm with high adhesion ability and resistance to the antimicrobial products, mainly due to the presence of extracellular matrix [47]. The ability of a doped composite resin inhibits the formation and adhesion of a mature biofilm could play an important role in the prevention of secondary caries.

A dental composite resin should have satisfactory mechanical properties besides the antibacterial activity to be accepted as a successful restorative dental material, especially in positions with heavily occlusal stresses [21]. The mechanical property which was evaluated in the current study includes the compressive strength.

The results showed that the incorporation of ZnO/Ag nanoplates into the composite resin did not significantly change the compressive strength in comparison to undoped composite resin. Otherwise, the doped composite resin with 1 and 2% of ZnO/Ag nanospheres decreased the compressive strength mean values (Fig. 12). Hojati et al. [21] related that the inclusion of small amounts (1%) of ZnO NPs into flowable composite resin could significantly increase the compressive strength and could not adversely affect other mechanical properties. Previous studies reported that incorporation of different nanoparticles into a composite resin leads to mechanical improvement [39,40,48]. In this study, the nanoparticles were not previously treated with silane agents, which may decrease the compressive strength of the composite resin. Nanoparticles surface modification with silanization agents leads to better dispersion and linkage of modified particles with resin matrix and could improve mechanical properties of dental resin based-composites [48]. Probably, the aggregated nanoplates allowed better linkage with resin matrix than nanospheres, which leads to no significant differences on the mechanical property for ZCS group.

The results demonstrated that ZnO/Ag nanoparticles inhibit *S. mutans* biofilm on the surface of the composite resin without significant changes on compressive strength with ZnO/Ag nanoplates, probably due the great homogeneity of NPs into the composite resin and the small amount incorporated (Figs. 12 and 13). We suggest that the antibacterial effect of this material is mainly due to the synergetic effect between ZnO and Ag nanoparticles, which is expected a higher formation of oxygen reactive species than the individual materials. These findings could help us to formulate a nanofilled restorative material with antibacterial activity. The state of the art of the currently commercial composite resins is represented by the inclusion of nanoparticles as filler content, however none of them has the ability to prevent biofilm formation on the surface of these resins. Therefore, the possibility to obtain an antibacterial nanofilled restorative material can provides esthetics restorations with greater longevity than conventional composite resins.

5. Conclusion

The inclusion of small amounts of Ag/ZnO NPs in nanoplates shape slightly increase compressive strength of the composite resin. Spherical nanoparticles of Ag/ZnO were able to significantly inhibit *S. mutans* biofilm cells over the composite resin surface. A reduced adhesion of

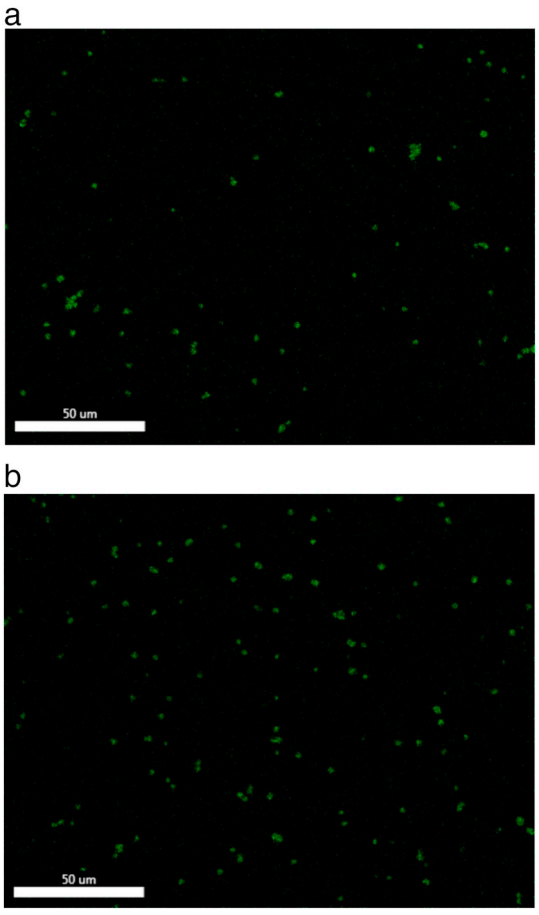

Fig. 13. EDX Zn map of the composite resin containing (a) 1% and (b) 2% of Ag/ZnO-NPs (ZCS). Green spots represent Zn element. (For interpretation of the references to color in this figure legend, the reader is referred to the web version of this article.)

the biofilm on resin surface was also noted when the resin was modified by the nanoparticles. Based on these results, the use of Ag/ZnO nanoparticles as filler content could be a good option to develop a new dental restorative resin based material with antibacterial properties.

Acknowledgments

The authors thank to the Coordination for the Improvement of Higher Education Personnel (CAPES) and Foundation for Research Support of the State of Amazonas (FAPEAM) for the financial support for this investigation.

References

[1] I. Nedeljkovic, W. Teughels, J. De Munck, B. Van Meerbeek, K.L. Van Landuyt, Is secondary caries with composites a material-based problem? Dent. Mater. 31 (2015) e247–e277, https://doi.org/10.1016/j.dental.2015.09.001.
[2] R. Chauhan, Good short-term survival rates for posterior resin composite restorations, Evid. Based Dent. 16 (2015) 114–115, https://doi.org/10.1038/sj.ebd.6401135.
[3] T. Beazoglou, S. Eklund, D. Heffley, J. Meiers, L.J. Brown, H. Bailit, Economic impact of regulating the use of amalgam restorations, Public Health Rep. (Washington, D.C. 1974) 122 (2007) 657.
[4] B.S. Lim, J.L. Ferracane, R.L. Sakaguchi, J.R. Condon, Reduction of polymerization contraction stress for dental composites by two-step light-activation, Dent. Mater. 18 (2002) 436–444, https://doi.org/10.1016/S0109-5641(01)00066-5.
[5] J.W. Park, C.W. Song, J.H. Jung, S.J. Ahn, J.L. Ferracane, The effects of surface roughness of composite resin on biofilm formation of *Streptococcus mutans* in the presence of saliva, Oper. Dent. 37 (2012) 532–539, https://doi.org/10.2341/11-371-L.
[6] S.P. Samuel, S. Li, I. Mukherjee, Y. Guo, A.C. Patel, G. Baran, Y. Wei, Mechanical properties of experimental dental composites containing a combination of mesoporous and nonporous spherical silica as fillers, Dent. Mater. 25 (2009) 296–301, https://doi.org/10.1016/j.dental.2008.07.012.
[7] Y.J. Wei, N. Silikas, Z.T. Zhang, D.C. Watts, Hygroscopic dimensional changes of self-adhering and new resin-matrix composites during water sorption/desorption cycles, Dent. Mater. 27 (2011) 259–266, https://doi.org/10.1016/j.dental.2010.10.015.
[8] S.C. Bayne, J.Y. Thompson, E.J. Swift, P. Stamatiades, M. Wilkerson, A characterization of first-generation flowable composites, J. Am. Dent. Assoc. 129 (1998) 567–577, https://doi.org/10.14219/jada.archive.1998.0274.
[9] J.L. Drummond, M.S. Bapna, Static and cyclic loading of fiber-reinforced dental resin, Dent. Mater. 19 (2003) 226–231, https://doi.org/10.1016/S0109-5641(02)00034-9.
[10] J.L. Ferracane, Resin composite—state of the art, Dent. Mater. 27 (2011) 29–38, https://doi.org/10.1016/j.dental.2010.10.020.
[11] Y. Hosoya, T. Shiraishi, T. Odatsu, J. Nagafuji, M. Kotaku, M. Miyazaki, J.M. Powers, Effects of polishing on surface roughness, gloss, and color of resin composites, J. Oral Sci. 53 (2011) 283–291, https://doi.org/10.2334/josnusd.53.283.
[12] N. Beyth, A.J. Domb, E.I. Weiss, An in vitro quantitative antibacterial analysis of amalgam and composite resins, J. Dent. 35 (2007) 201–206, https://doi.org/10.1016/j.jdent.2006.07.009.
[13] B.A. Sevinç, L. Hanley, Antibacterial activity of dental composites containing zinc oxide nanoparticles, J. Biomed. Mater. 94 (2010) 22–31, https://doi.org/10.1002/jbm.b.31620.Antibacterial.
[14] M. Kawashita, S. Tsuneyama, F. Miyaji, T. Kokubo, H. Kozuka, K. Yamamoto, Antibacterial silver-containing silica glass prepared by sol-gel method, Biomaterials 21 (2000) 393–398, https://doi.org/10.1016/S0142-9612(99)00201-X.
[15] Y. Zhang, X. Gao, L. Zhi, X. Liu, W. Jiang, Y. Sun, J. Yang, The synergetic antibacterial activity of Ag islands on ZnO (Ag/ZnO) heterostructure nanoparticles and its mode of action, J. Inorg. Biochem. 130 (2014) 74–83, https://doi.org/10.1016/j.jinorgbio.2013.10.004.
[16] S. Kasraei, L. Sami, S. Hendi, M.-Y. Alikhani, L. Rezaei-Soufi, Z. Khamverdi, Antibacterial properties of composite resins incorporating silver and zinc oxide nanoparticles on *Streptococcus mutans* and *Lactobacillus*, Restor. Dent. Endod. 39 (2014) 109–114, https://doi.org/10.5395/rde.2014.39.2.109.
[17] V. Uskoković, L.E. Bertassoni, Nanotechnology in dental sciences: moving towards a finer way of doing dentistry, Materials (Basel) 3 (2010) 1674–1691, https://doi.org/10.3390/ma3031674.
[18] M.A.S. Melo, S.F.F. Guedes, H.H.K. Xu, L.K.A. Rodrigues, Nanotechnology-based restorative materials for dental caries management, Trends Biotechnol. 31 (2013) 459–467, https://doi.org/10.1016/j.tibtech.2013.05.010.
[19] J.L. Ferracane, Current trends in dental composites, Crit. Rev. Oral Biol. Med. 6 (1995) 302–318, https://doi.org/10.1177/10454411950060040301.
[20] J. Jin, G. Wei, A. Hao, W. Zhang, Y. Zhang, Q. Wang, Q. Chen, ZnO–AlBw-reinforced dental resin composites: the effect of pH level on mechanical properties, RSC Adv. 5 (2015) 26430–26437, https://doi.org/10.1039/C5RA01413A.
[21] S.T. Hojati, H. Alaghemand, F. Hamze, F. Ahmadian Babaki, R. Rajab-Nia, M.B. Rezvani, M. Kaviani, M. Atai, Antibacterial, physical and mechanical properties of flowable resin composites containing zinc oxide nanoparticles, Dent. Mater. 29 (2013) 495–505, https://doi.org/10.1016/j.dental.2013.03.011.
[22] M. Fang, J.H. Chen, X.L. Xu, P.H. Yang, H.F. Hildebrand, Antibacterial activities of inorganic agents on six bacteria associated with oral infections by two susceptibility tests, Int. J. Antimicrob. Agents 27 (2006) 513–517, https://doi.org/10.1016/j.ijantimicag.2006.01.008.
[23] L.K. Adams, D.Y. Lyon, A. McIntosh, P.J.J. Alvarez, Comparative toxicity of nanoscale TiO2, SiO2 and ZnO water suspensions, Water Sci. Technol. 2006, pp. 327–334, , https://doi.org/10.2166/wst.2006.891.
[24] R.P. Allaker, The use of nanoparticles to control oral biofilm formation, J. Dent. Res. 89 (2010) 1175–1186, https://doi.org/10.1177/0022034510377794.
[25] J. Min Peng, J. Cheng Lin, Z. Yu Chen, M. Chao Wei, Y. Xiang Fu, S. Shen Lu, D. Sheng Yu, W. Zhao, Enhanced antimicrobial activities of silver-nanoparticle-decorated reduced graphene nanocomposites against oral pathogens, Mater. Sci. Eng. C 71 (2017) 10–16, https://doi.org/10.1016/j.msec.2016.09.070.
[26] C. Takahashi, N. Matsubara, Y. Akachi, N. Ogawa, G. Kalita, T. Asaka, M. Tanemura, Y. Kawashima, H. Yamamoto, Visualization of silver-decorated poly (DL-lactide-co-glycolide) nanoparticles and their efficacy against *Staphylococcus epidermidis*, Mater. Sci. Eng. C Mater. Biol. Appl. 72 (2017) 143–149, https://doi.org/10.1016/j.msec.2016.11.051.
[27] S. Ghosh, V.S. Goudar, K.G. Padmalekha, S.V. Bhat, S.S. Indi, H.N. Vasan, ZnO/Ag nanohybrid: synthesis, characterization, synergistic antibacterial activity and its mechanism, RSC Adv. 2 (2012) 930, https://doi.org/10.1039/c1ra00815c.
[28] A.B.P. Jiménez, C.A.H. Aguilar, J.M.V. Ramos, P. Thangarasu, Synergistic antibacterial activity of nanohybrid materials ZnO-Ag and ZnO-Au: synthesis, characterization, and comparative analysis of undoped and doped ZnO nanoparticles, Aust. J. Chem. 68 (2015) 288–297, https://doi.org/10.1071/CH14123.
[29] L. Cheng, K. Zhang, M.D. Weir, M.A.S. Melo, X. Zhou, H.H.K. Xu, Nanotechnology strategies for antibacterial and remineralizing composites and adhesives to tackle dental caries, Nanomedicine (London) 10 (2015) 627–641, https://doi.org/10.2217/nnm.14.191.
[30] E.D. Cavassin, L.F.P. de Figueiredo, J.P. Otoch, M.M. Seckler, R.A. de Oliveira, F.F. Franco, V.S. Marangoni, V. Zucolotto, A.S.S. Levin, S.F. Costa, Comparison of methods to detect the in vitro activity of silver nanoparticles (AgNP) against multidrug resistant bacteria, J. Nanobiotechnol. 13 (2015) 64, , https://doi.org/10.1186/s12951-015-0120-6.
[31] E.R. Leite, M.I.B. Bernardi, E. Longo, J.A. Varela, C.A. Paskocimas, Enhanced electrical property of nanostructured Sb-doped SnO2 thin film processed by soft

chemical method, Thin Solid Films 449 (2004) 67–72, https://doi.org/10.1016/j.tsf.2003.10.101.
[32] Y. Jia, X.-Y. Yu, T. Luo, M.-Y. Zhang, J.-H. Liu, X.-J. Huang, PEG aggregation templated porous ZnO nanostructure: room temperature solution synthesis, pore formation mechanism, and their photoluminescence properties, CrystEngComm 15 (2013) 3647, https://doi.org/10.1039/c3ce27091b.
[33] P.B.A. das Neves, J.A.M. Agnelli, C. Kurachi, C.W.O. de Souza, Addition of silver nanoparticles to composite resin: effect on physical and bactericidal properties in vitro, Braz. Dent. J. 25 (2014) 141–145, https://doi.org/10.1590/0103-6440201302398.
[34] K.L. Kelly, E. Coronado, L.L. Zhao, G.C. Schatz, The optical properties of metal nanoparticles: the influence of size, shape, and dielectric environment, J. Phys. Chem. B 107 (2003) 668–677, https://doi.org/10.1021/jp026731y.
[35] K.S.W. Sing, D.H. Everett, R.a.W. Haul, L. Moscou, R.a. Pierotti, J. Rouquérol, T. Siemieniewska, Reporting physisorption data for gas/solid systems with special reference to the determination of surface area and porosity (Recommendations 1984), Pure Appl. Chem. 57 (1985) 603–619, https://doi.org/10.1351/pac198557040603.
[36] M.P. Pechini, N. Adams, Method of Preparing Lead and Alkaline Earth Titanates and Niobates and Coating Method Using the Same to Form a Capacitor, United States Pat. Off., 1967, pp. 01–07.
[37] R.S. Razavi, M.R. Loghman-estarki, M. Farhadi-khouzani, Synthesis and characterization of ZnO nanostructures by polymeric precursor route, 121 (2012) 98–100.
[38] S.M. Dizaj, F. Lotfipour, M. Barzegar-Jalali, M.H. Zarrintan, K. Adibkia, Antimicrobial activity of the metals and metal oxide nanoparticles, Mater. Sci. Eng. C 44 (2014) 278–284, https://doi.org/10.1016/j.msec.2014.08.031.
[39] J. Sun, A.M. Forster, P.M. Johnson, N. Eidelman, G. Quinn, G. Schumacher, X. Zhang, W.L. Wu, Improving performance of dental resins by adding titanium dioxide nanoparticles, Dent. Mater. 27 (2011) 972–982, https://doi.org/10.1016/j.dental.2011.06.003.
[40] Y. Hua, L. Gu, H. Watanabe, Micromechanical analysis of nanoparticle-reinforced dental composites, Int. J. Eng. Sci. 69 (2013) 69–76, https://doi.org/10.1016/j.ijengsci.2013.04.001.
[41] L.F. Espinosa-Cristóbal, G.A. Martínez-Castañón, R.E. Martínez-Martínez, J.P. Loyola-Rodríguez, N. Patiño-Marín, J.F. Reyes-Macías, F. Ruiz, Antibacterial effect of silver nanoparticles against *Streptococcus mutans*, Mater. Lett. 63 (2009) 2603–2606, https://doi.org/10.1016/j.matlet.2009.09.018.
[42] A.E. Nel, L. Mädler, D. Velegol, T. Xia, E.M.V. Hoek, P. Somasundaran, F. Klaessig, V. Castranova, M. Thompson, Understanding biophysicochemical interactions at the nano-bio interface, Nat. Mater. 8 (2009) 543–557, https://doi.org/10.1038/nmat2442.
[43] M.Z. Kassaee, A. Akhavan, N. Sheikh, A. Sodagar, Antibacterial effects of a new dental acrylic resin containing silver nanoparticles, J. Appl. Polym. Sci. 110 (2008) 1699–1703, https://doi.org/10.1002/app.
[44] H. Jia, W. Hou, L. Wei, B. Xu, X. Liu, The structures and antibacterial properties of nano-SiO2 supported silver/zinc-silver materials, Dent. Mater. 24 (2008) 244–249, https://doi.org/10.1016/j.dental.2007.04.015.
[45] Y. Jiang, L. Zhang, D. Wen, Y. Ding, Role of physical and chemical interactions in the antibacterial behavior of ZnO nanoparticles against *E. coli*, Mater. Sci. Eng. C 69 (2016) 1361–1366, https://doi.org/10.1016/j.msec.2016.08.044.
[46] Z. Wang, Y. Shen, M. Haapasalo, Dental materials with antibiofilm properties, Dent. Mater. 30 (2014) e1–e16, https://doi.org/10.1016/j.dental.2013.12.001.
[47] R.M. Donlan, Biofilms: microbial life on surfaces, Emerg. Infect. Dis. 8 (2002) 881–890, https://doi.org/10.3201/eid0809.020063 http://www.cdc.gov/ncidod/EID/vol8no9/02-0063.htm.
[48] Y. Xia, F. Zhang, H. Xie, N. Gu, Nanoparticle-reinforced resin-based dental composites, J. Dent. 36 (2008) 450–455, https://doi.org/10.1016/j.jdent.2008.03.001.